Recent Progress in First Principles Investigations of Magnetism of Surfaces and Thin Films

Ruqian Wu

Department of Physics & Astronomy, California State University,

Northridge, CA 91330-8268, USA

and

A. J. Freeman

Department of Physics & Astronomy, Northwestern University,

Evanston, IL 60208-3112, USA

Abstract

The present state of the art of theoretical studies of magnetism in artificial low dimensional transition metal materials, e.g., surfaces, overlayers and multilayers, is reviewed here by means of some illustrative examples. Strong magnetic moment enhancements are found for Fe, Co and Ni atoms at surfaces or interfaces contacting with inert substrates. By contrast, the spin polarization is strongly frustrated in systems with strong hybridization, which usually leads to more complex antiferromagnetic ground states. As a major progress for first principles determination of the magneto-crystalline anisotropy, the state tracking and the torque approaches enable us to obtain very stable and reliable results of the MCA energy and other subsequent effects such as magnetostriction. The x-ray magnetic circular dichroism and its application for determination of spin, orbital and dipole moments at surfaces and interfaces are also discussed.

1 Introduction

As Allan Mackintosh understood and applauded, magnetism research has been undergoing a renaissance over the last decade following the discovery of a variety of new scientific phenomena associated with man-made transition metal thin films. Among them are the theoretical prediction of enhanced magnetic moments in ultrathin films and at surfaces (Freeman et al., 1991), the discovery of perpendicular magnetic anisotropy (Garcia et al., 1985) in layered structures, and the discovery of giant magnetoresistance (GMR, Baibich et al., 1988 and Binasch et al., 1989) and accompanying oscillatory exchange coupling in multilayers made by alternating magnetic and "nonmagnetic" metals (Parkin et al., 1990). Some of these discoveries

are expected to have a major impact on the magnetic recording industry. An example is the so-called spin-valve sensor (Dieny et al., 1991), which is about to be used as a magnetic recording head. Other applications are multilayers with out-of-plane anisotropy which show promise as "blue" magneto-optical media (Hurst et al., 1993), or GMR based structures which offer non-volatile alternatives to semiconductor based DRAM (Daughton et al., 1992).

As was also known to him, the great success of first principles electronic structure studies based on local spin density functional theory, which performs extremely complex simulations of ever increasingly realistic systems, plays a very important role in explaining magnetism in thin films and has led to the facing of even more challenging problems (Freeman et al., 1991). Theoretical calculations predicted the large enhancement of the magnetic moment for $3d$ transition metal (TM) surfaces or overlayers deposited on inert substrates, and the possible magnetization in some normally non-magnetic materials – for which some results have already been verified experimentally. Complex magnetic structures, especially some antiferromagnetic (AFM) configurations, can now be predicted by comparing total energies with their equilibrium atomic geometries (including multilayer relaxations and reconstructions at surfaces and interfaces) optimized very efficiently using the atomic force approach. Significant progress has been made very recently for the treatment of the weak spin-orbit coupling (SOC) and now we are able to obtain (i) very reliable results for the magneto-crystalline anisotropy (MCA) energies and magnetostrictive coefficients for transition metal thin films using the state tracking (Wang et al, 1993) and the torque (Wang et al., 1996) approaches; (ii) magneto-optical Kerr effect (MOKE) and soft x-ray magnetic circular dichroism (MCD). Using a linear response theory, magnetic transport properties, such as GMR, can also be determined from the ground state band structures.

The aim of the present review, dedicated to Allan Mackintosh, is to present the main lines of important theoretical developments in this exciting area in recent years with an emphasis on our own full potential linearized augmented plane wave (FLAPW) (Wimmer et al., 1981) calculations. Examples presented here indicate that high quality *ab initio* calculations of magnetic systems can achieve high accuracy/precision for a wide range of magnetic properties of transition metal and rare-earth metal systems. The new level of performance and the capability of modern computational simulations can help to alleviate many expensive experimental procedures, and can gradually build up effective tools to search for new magnetic materials.

2 3*d* Overlayers

As determined by Hund's rules, most of the free transition metal atoms possess a net spin moment. In the solid state, their magnetic moments decrease because the interatomic Coulomb repulsion diminishes the parallel spin alignment in the region between the atoms. Naturally, a reduced dimensionality, e.g., in 2D (i.e., monolayer) or 1D (i.e., linear chain) systems, is expected to restore the free atom nature of the atom in question and thus to enhance the local magnetic moment. Indeed, the calculated magnetic moments of 3*d* transition metals increase with the decreasing dimensionality of system in going from bulk, surface and to a free monolayer (Freeman et al., 1991).

To realize the predicted strong magnetic moment in monolayers, supporting substrates should be lacking electronic states at the Fermi energy so as to minimize the overlayer-substrate hybridization. As listed in Table I, the magnetic moments of Fe and Co atoms are reduced by only about 0.1–0.2 μ_B on Ag(001) or Au(001) compared to those in their free-standing monolayers. Surprisingly, Cu(001) exhibits very strong proximity effects; the overlayer magnetic moments are reduced by 0.5 μ_B from those in the free standing case. A benign substrate, namely MgO(001), was found on which the spin moment of an Fe monolayer is as large as 3.07 μ_B – almost unchanged from the value for the free standing Fe monolayer, 3.10 μ_B. Since MgO(001) has no states in the gap at E_F even for the surface layer, Fe/MgO(001) is almost free of chemical interactions.

With strong interfacial interactions, e.g., in Fe/W(001) and Fe/Ru(0001), we found that AFM ordering prevails since the FM state is frustrated by the *d*-band hybridization. For example, Fe/W(001) has no stable, or even metastable, FM states. By contrast, the AFM state ($M = 0.7\ \mu_B$) is about 0.01 eV/cell lower than the PM state. Very interestingly, the FM ordering of the "dead" Fe layer can be activated by an additional Fe overlayer and the magnetic moments in the interface and surface layers jump to 1.68 μ_B and 2.43 μ_B, respectively. Therefore, the observations of magnetism in Fe/W(001) should vary dramatically between one and two layers.

On the diamond (001) surface, we found that a large Fe and Co magnetic moment can be sustained (1.93 μ_B and 1.56 μ_B, respectively), whereas the magnetic moment of a Ni monolayer is reduced to zero. It was found that the magnetic moments strongly depend on the interlayer distance due to the interaction with the dangling bond surface states on C(001). Interestingly, Fe and Co magnetic layers induce almost zero magnetic moments at the interfacial C sites and a sizable magnetic moment at the subinterfacial C sites (0.04 μ_B).

A strong interplay between magnetism and atomic structure was found for Mn/Fe(001). The antiparallel alignment in the Mn plane with a large (3.1 μ_B)

Table I. Magnetic moment (μ_B) and magnetic ground state of magnetic monolayer and overlayer systems.

System	Monolayer		Overlayer	
	state	moment	state	moment
Fe/Ag(001)	FM	3.20-3.4	FM	2.96-3.01
Fe/Au(001)	FM	–	FM	2.97
Co/Ag(001)	FM	2.20	FM	2.03
Ni/Ag(001)	FM	1.02	FM	0.57-0.65
Fe/MgO(001)	FM	3.10	FM	3.07
Fe/Cu(001)	FM	3.20	FM	2.69-2.85
Co/Cu(001)	FM	2.05	FM	1.79
Ni/Cu(001)	FM	1.01	FM	0.39
Ni/Cu(111)	FM	1.01	FM	0.34
Fe/C(001)	FM	2.96	FM	1.93
Co/C(001)	FM	2.06	FM	1.56
Ni/C(001)	FM	1.03	PM	0.00
Pd/Ag(001)	FM	0.40	PM	0.00
Pd/MgO(001)	FM	0.34	PM	0.00
Pd/C(0001)	FM	0.14	PM	0.00
Rh/Au(001)	FM	1.56	FM	1.09
Rh/Ag(001)	FM	1.45	FM	0.95
Rh/MgO(001)	FM	1.45	FM	1.21
Rh/C(0001)	FM	1.35	FM	0.24
Ru/Ag(001)	FM	2.12	FM	1.57
Ru/MgO(001)	FM	2.14	FM	1.95
Ru/C(0001)	FM	2.48	FM	0.28
Fe/W(110)	FM	2.98	FM	2.18
Fe/W(001)	FM	3.10	AFM	0.93
Fe/Ru(0001)	FM	2.90	AFM	2.23
Mn/Fe(001)	AFM	4.32	AFM	3.15

magnetic moment is found to drive a $c(2 \times 2)$ buckling reconstruction in the Mn overlayer. Due to hybridization with the magnetic Fe(001) substrate, the valence bands of the two different Mn atoms differ substantially and thus FM signals can be detected from the AFM Mn monolayer using techniques such as spin-polarized photoemission. For the bilayer Mn/Fe(001) (i.e., 2Mn/Fe(001)), we found that the surface Mn layer (instead of the interfacial Mn layer) appears to couple antiferromagnetically with the underlying Fe substrate. This unusual behaviour was also found in experiments for Cr/Fe(001) and Mn/Fe(001) (Roth et al., 1995). Again, we found that the magnetic ordering in 2Mn/Fe(001) is very sensitive to the atomic structure and thus the positions of all the atoms need to be well optimized for such

a system.

3 Possible 4*d* magnetism

It was found that some 4*d* elements, namely Pd, Rh and Ru, can possess magnetic moments in certain circumstances. In an isolated monolayer geometry, the calculated magnetic moments for Pd, Rh and Ru are 0.35 μ_B, 1.45 μ_B and 2.12 μ_B, respectively (Zhu et al., 1990; Wu et al., 1992). Physically, the density of states at E_F of paramagnetic Ru and Rh monolayers is found to increase by 450% over their corresponding bulk values, which results in a large Stoner factor (1.45 and 1.89 for Ru and Rh monolayers, respectively) and thus a Stoner instability.

Strikingly, the magnetism of the free Rh monolayer is found to remain when placed on Ag(001) and Au(001) substrates. However, verification experiments using the surface magneto-optic Kerr effect (SMOKE) failed to find any evidence of ferromagnetism in Rh/Ag(001) at temperatures down to 40 K. (Mulhollan et al., 1991; Liu et al., 1992). To understand this discrepancy, FLAPW calculations were carried out for the Rh/Ag(001), Ru/Ag(001), Ag/Rh/Ag(001) and Ag/Ru/Ag(001) systems. The overlayer relaxation is found to be very small and to have no significant effect on the electronic and magnetic properties. Further, we found that the ferromagnetism of Rh/Ag(001) can be destroyed by an additional Ag layer – which attributes the lack of ferromagnetism in recent SMOKE experiments to the surface segregation between Rh and Ag atoms. By contrast, Ru/Ag(001) is predicted to be ferromagnetic with both a larger magnetic moment and larger magnetic energy even after being covered by a Ag layer, and thus is more suitable for experimental verification. In addition, the considerably stronger overlayer-substrate Coulomb repulsion indicates that Ag is no longer the "benign" substrate for 4*d* overlayer magnetism that it is for the 3*d* metals.

As expected, large magnetic moments are predicted for Ru and Rh monolayers on MgO(001) (1.95 μ_B and 1.21 μ_B for Ru and Rh, respectively) – indicating, in principle, the potential application of MgO(001) as a benign substrate for 4*d* monolayer magnetism. Significantly, according to our atomic force determinations, the metal overlayers induce a sizable *buckling* reconstruction in the interfacial MgO layer, which enhances the M–MgO binding energy by 0.1 eV. The weak M–O interaction is mainly via tail effects; however, it affects the density of states at the Fermi level for Pd/MgO(001) significantly and completely eliminates the small magnetic moment of the free Pd monolayer (0.34 μ_B).

A nonzero in-plane spin polarization was observed for Ru/C(0001) below 250 K, using spin-polarized secondary electron emission (SPSEE) techniques (Pfandzelter et al., 1995). This first evidence of 4*d* monolayer magnetism is very encouraging and

deserves theoretical verification. Surprisingly, the calculated magnetic moments of Rh/C(0001) and Ru/C(0001) are only 0.24 μ_B/adatom and 0.28 μ_B/adatom even in a very sparse structure. Furthermore, the magnetic moments are found to depend strongly on the overlayer/substrate interlayer distance. The calculated magnetic moment of Ru jumps discontinuously to a value as large as 1.1 μ_B just slightly away from the equilibrium position. It can even reach a value of 1.5 μ_B if the interlayer distance is 10% larger than the equilibrium one. Such a discontinuous behaviour suggests the co-existence of several high- and low-spin moment states.

4 Magneto-crystalline anisotropy

As is known, the strength of spin-orbit coupling (SOC) in $3d$ transition metal systems is very weak (30–50 meV, or 100 times smaller than that of the crystalline field) and thus can be well treated using a perturbative framework. As stated in the often-used MCA force theorem, the MCA energy can be approximately taken as the *band* energy

$$E_{\mathrm{MCA}} = E(\rightarrow) - E(\uparrow) = \sum_{\mathrm{occ}'} \varepsilon_i(\rightarrow) - \sum_{\mathrm{occ}''} \varepsilon_i(\uparrow) + O(\delta\rho^n)\,. \tag{1}$$

Very recently, we proved that the order of n goes up to 4 for thin film systems, and thus the force theorem should be able to provide sufficient accuracy for MCA energy determinations. However, several numerical uncertainties have been inherent in most previous *ab initio* MCA calculations because the sets of occupied states, i.e., $\{\mathrm{occ}'\}$ and $\{\mathrm{occ}''\}$, were determined through the Fermi filling scheme which relies on the very limited information from the eigenvalues, ε_i.

Recently, we proposed the state tracking approach in which the $\{\mathrm{occ}'\}$ and $\{\mathrm{occ}''\}$ states are determined according to their projections back to the occupied set of the unperturbed states. Since this procedure ensures minimum change in the charge and spin densities as required by the force theorem and excludes the possible randomness in the Brillouin zone (tracking at a given k-point) (Wang et al., 1993), very stable MCA results have been obtained for magnetic thin films such as Fe, Co and Ni monolayers in the free standing case as well as on various substrates (Cu and Pd, etc) with relatively small number of k-points. Perhaps more importantly, the behaviour of MCA for transition metal thin films can now be related to more fundamental properties, such as band structures and wave functions. This enables us to explore the underlying physics and, furthermore, to figure out a way to tune the MCA for transition metal systems: For example, the strong in-plane MCA of a free standing Co monolayer is found to originate from the coupling between the occupied $d_{xz,yz}$ and unoccupied d_{z^2} and $d_{x^2-y^2}$ states at the $\bar{M}$ point. When adsorbed onto the Cu substrate, for example, the $d_{xz,yz}$ state is lowered in energy

due to the interfacial hybridization and thus the MCA energy becomes less negative in the Co/Cu overlayer systems and even positive in Co/Cu sandwiches.

More recently, we proposed a torque (Wang et al., 1996) method which can further depress the remaining uncertainties resulting from the SOC interaction between near-degenerate states around the Fermi level (so called surface pair coupling). To demonstrate the idea of the torque method, recall that the total energy of an uniaxial system can be well approximated in the form

$$E = E_0 + K_2 \sin^2\theta + K_4 \sin^4\theta\,, \tag{2}$$

where θ is the angle between the normal axis and the direction of magnetization. It is easy to find that the MCA energy is equal to the angular derivative of the total energy (torque) at a "magic angle" of $\theta = 45°$ as

$$E_{\mathrm{MCA}} \equiv E(\theta = 90°) - E(\theta = 0°) = K_2 + K_4 = dE/d\theta\big|_{\theta=45°}\,. \tag{3}$$

If we apply the Feynman-Hellman theorem, E_{MCA} can be evaluated finally as (note only $H^{\mathrm{soc}} = \xi\ \mathbf{s}\cdot\mathbf{L}$ depends on θ in the Hamiltonian)

$$E_{\mathrm{MCA}} = \sum_{\mathrm{occ}} \langle \Psi_i' | dH/d\theta | \Psi_i' \rangle\big|_{\theta=45°} = \sum_{\mathrm{occ}} \langle \Psi_i' | \partial H^{\mathrm{soc}}/\partial\theta | \Psi_i' \rangle\big|_{\theta=45°} \tag{4}$$

where Ψ_i' is the ith perturbed wave function.

The advantage of the torque method is obvious since in this approach we only have to deal with one particular magnetic orientation and thus only one Fermi surface is required for the k-integration. In addition, the MCA energy is expressed as the expectation value of the angular derivative of H^{soc} and therefore it is much more insensitive to the surface pair coupling. With the aid of the state tracking and torque methods, very stable results have been obtained for various transition metal systems and so we are able to attack the long standing problem of magnetostriction in transition metals.

As a first illustration, consider isolated monoatomic iron and cobalt layers with the same square lattice so that their electronic bands are very similar. Despite these similarities, in-plane and perpendicular surface MCA are expected for Co and Fe, respectively, from both experiment and theoretical calculations. According to our calculation and analysis, this is caused by the different occupation of the spin-down d bands due to the difference in the valence electron number. For example, for the Co monolayer, two bands consisting of xz and yz states are all occupied in a large region near $\bar{M}$. They are coupled through either l_y or l_x angular momentum components to the empty z^2 states, and this contributes to the in-plane MCA. The variation of the surface MCA for different atomic (Co vs Fe) layers amounts to about 3 meV, depending on the lattice strain.

In an overlayer system, the MCA energy depends mainly on the hybridization between its out-of-plane states, namely the xz and yz states, and the orbitals of the substrates. At the Co–Pd interface of a Pd/Co/Pd sandwich, for example, the Co xz and yz states have been appreciably pushed up to higher energy which results in perpendicular interface MCA. We found that the effects of different substrates can affect the MCA energy by 2 to 3 meV. These interfacial effects are well described using an effective ligand interaction model.

5 Magnetostriction

In general, the size of the (magnetostrictive) strain induced by rotation of the magnetization of a magnetic material depends on the direction of the measured strain and magnetization with respect to the crystalline axes of the material. For a cubic material, the directional dependence of the fractional change in length can be expressed in terms of the direction cosines of the magnetizations (α_i) and those of the measurement direction (β_i) with respect to the crystalline axes

$$\frac{\Delta l}{l} = \frac{3}{2}\lambda_{100}\Big[\sum_{i=1}^{3}\alpha_i^2\beta_i^2 - \frac{1}{3}\Big] + 3\lambda_{111}\sum_{i\neq j}\alpha_i\alpha_j\beta_i\beta_j\,. \tag{5}$$

If the measurement is carried out along the (001) direction for example, $\beta_x = \beta_y = 0$ and $\beta_z = 1$, Eq. (5) can be simplified as

$$\frac{\Delta l}{l} = \frac{3}{2}\lambda_{100}\Big[\alpha_z^2 - \frac{1}{3}\Big] \tag{6}$$

and

$$\lambda_{100} = \frac{2}{3}\frac{\Delta l_z - \Delta l_{x,y}}{l}\,. \tag{7}$$

Clearly, λ_{100} represents the change in length along (001) when the magnetization turns from the the x–y plane to the z direction.

The equilibrium length l can be obtained by fitting the calculated total energy as a quadratic function of l ($l_0 = -b/2a$) as

$$E = al^2 + bl + c\,. \tag{8}$$

If the MCA energy is a linear function of l (as will be demonstrated)

$$E_{\mathrm{MCA}} = E(x,y) - E(z) = k_1 l + k_2 \tag{9}$$

then we finally have

$$\lambda_{001} = -2k_1/3b\,. \tag{10}$$

Obviously, while the value of b can be easily calculated with high precision, the bottleneck for the determination of λ is the value of k_1, i.e., the strain dependence of the MCA energy.

For cubic bulk magnetic transition metals, the in-plane lattice constants are expected to change when the strains are applied along the vertical direction. Here, we consider two modes of distortion, namely (i) constant volume (i.e., γ_1 mode) and (ii) constant area in the lateral plane, when we change l to determine the magnetostrictive coefficients. For the γ_1 mode, the calculated total energies and MCA energies are plotted in Fig. 1. For bulk bcc Fe and fcc Co and Ni, the total energy can be well-fitted by a parabola and the MCA energy exhibits a good linearity with respect to the change of l – indicating the high precision of the present calculations and also justifying the huge range of strain ($\Delta l/l \sim 5$–20%) used in the calculations relative to saturation magnetostrictive strains ($\Delta l/l \sim 10^{-5}$).

For both the constant volume and constant area modes, the calculated λ_{001} is *positive* for bcc Fe and fcc Co – meaning that the dimension expands along the direction of magnetization; by contrast, the calculated λ_{001} for bulk fcc Ni is opposite in sign. For the constant area mode, the values of λ_{001} decrease substantially from the results obtained for the constant volume mode. These zero temperature results are of the correct sign and set a satisfactory range for the measured values of λ_{001}. They thus serve to validate this new approach for determining the tiny magnetostriction in transition metal systems.

To extend this approach to thin films consisting of a magnetic monolayer and a thick non-magnetic substrate, one should bear in mind that the lattice constant in the lateral plane is fixed by the substrate and so only strains along the vertical direction can be observed. The l in Eqs. (8) and (9) should therefore be considered as the interlayer distance between the magnetic overlayer and the non-magnetic substrate. The orientation of the substrate is used as a subscript for λ, e.g., λ_{100} stands for systems with (100) substrates. To simulate Co/Cu(001) and Co/Pd(001), a slab consisting of seven ideally constructed fcc Cu or Pd layers ($a_{\mathrm{Cu}} = 6.83$ a.u. and $a_{\mathrm{Pd}} = 7.35$ a.u.) with a pseudomorphic Co overlayer on each side is used.

For each system, the total energy curve can be well fitted by a parabola and the MCA energy exhibits a fairly good linearity as functions of the overlayer/substrate distance. We found for Co/Cu(001) that b and k_1 are equal to -4390 meV/a.u. and -0.376 meV/a.u., respectively; thus, the calculated λ_{100} at the Co/Cu(001) interface is -5.7×10^{-5}. The negative sign means that the Co–Cu interlayer distance contracts when the direction of magnetization changes from in-plane to normal to the surface. Dramatically, we found that the MCA energy for Co/Pd(001) becomes more *negative* when the Co–Pd distance shrinks and thus λ_{001} becomes *positive*, $+2.3 \times 10^{-4}$, just opposite to that for Co/Cu(001).

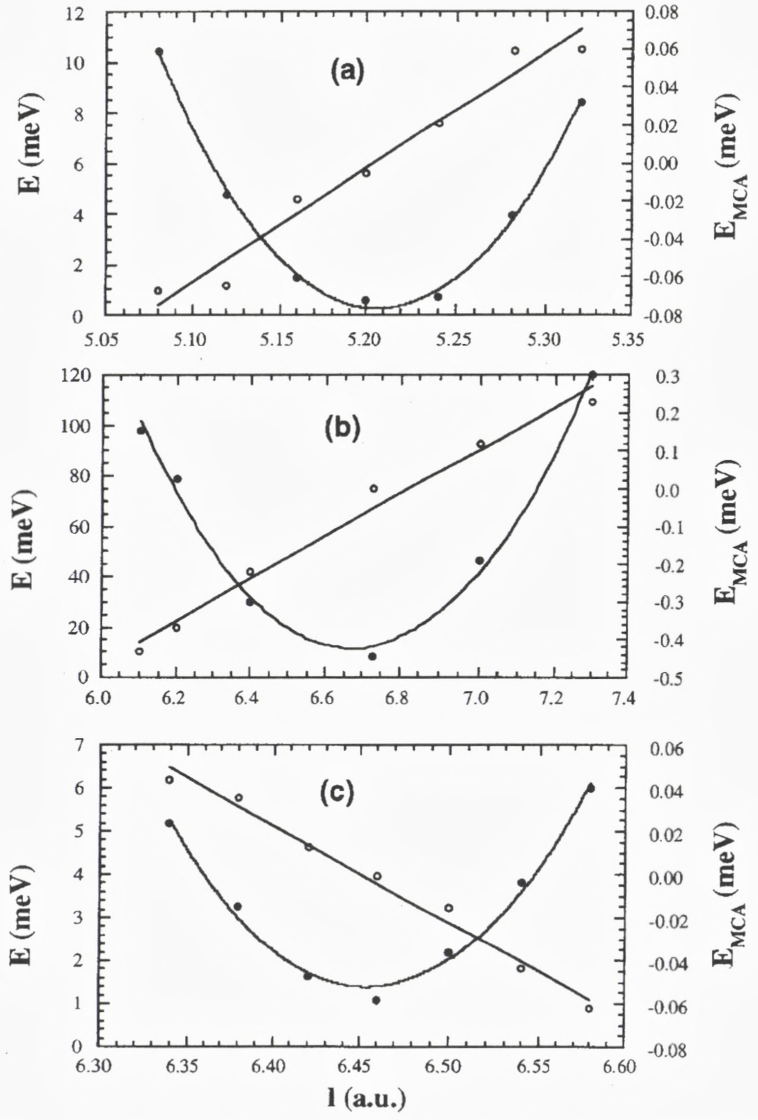

Figure. 1. The calculated total energy (left scale) and MCA energy (right scale) as a function of the length of the c-axis for (a) bcc Fe, (b) fcc Co and (c) fcc Ni.

6 Strain-induced MCA in Ni/Cu(001)

In many cases, the origin of perpendicular magnetic anisotropy (PMA) in ultra thin films is still not very clear today. It is believed that PMA originates from the altered hybridization, reduced symmetry or the stronger spin-orbit coupling (SOC) interaction at the interfacial region when heavier substrate atoms (Pd or Pt) are involved. It is hard, however, to explain the observation for Ni/Cu(001) in which the PMA occurs only when the Ni film becomes thicker than seven atomic layers (Baberschke, 1996). To understand this unusual result, we calculated the MCA energies of bulk fct Ni (lattice matched with Cu(001)) and of the mono- and bi-layer Ni/Cu(001) overlayer systems. We find that the lattice strain in bulk fct Ni leads to a large positive MCA energy (an inverse effect of magnetostriction), whereas the interfacial contribution to the MCA energy is negative (-1.1 meV per Ni atom). Thus, the PMA in Ni/Cu(001) is clearly due to strain-induced effects in the bulk, rather than interfacial effects, as was believed in the literature.

Similar to that in Fig. 1, the calculated MCA energies for bulk fct Ni can be well fitted by a linear function of the length of the c-axis. When c is equal to 6.83 a.u. (ideal fcc Cu lattice), the MCA energy is smaller than 1 μeV/atom – a result which indicates the precision of the present approach for the determination of the MCA energy for bulk magnetic transition metals. At the position corresponding to the measured structure ($c = 6.44$ a.u.), the MCA energy reaches 65 μeV/atom. This result agrees well with recent experimental data extrapolated to zero temperature, i.e., 70 μeV/atom (Baberschke, 1996). In bulk fct Ni, with a magnetic moment of 0.65 μ_B, the calculated shape (so-called volume) anisotropy energy due to the magnetostatic dipole interactions is less than 0.6 μeV/atom for a wide range of lattice distortion (10%). Thus, the MCA contribution is the dominant part of the PMA.

The strain-induced MCA energy is found to originate from the shift of the unoccupied $d_{xz,yz}$ states ($m = 1$) into a higher energy region when the lattice is compressed along the vertical direction. This weakens the spin-orbit interactions between the $d_{xz,yz}$ and the occupied non-bonding $d_{x^2-y^2}$ and d_{z^2} states (which yield a negative MCA energy). Meanwhile, almost no change is found for the unoccupied states with $m = 2$ and $m = 0$. The SOC interactions between the $d_{x^2-y^2}$ and d_{xy} states (which give a positive MCA energy) are therefore almost unaffected. This results in a positive MCA energy since the SOC interactions with the same m prevail over that with different m.

We have also determined the MCA energies of mono- and bi-layer Ni/Cu(001) thin films; they are -0.69 meV/atom and -0.30 meV/atom, respectively. Again, the shape anisotropy is negligible even for these overlayer systems (e.g., it is 0.023 meV/atom for the monolayer Ni/Cu(001)). The net MCA energy is strongly nega-

tive so that in-plane magnetization is preferred for the ultra-thin overlayer system. Thus, at least for Ni/Cu(001), the observed PMA for thick overlayers does not come from surface/interface effects as was believed before, but appears to be due to the strain-induced bulk contribution.

7 MCD at surfaces and interfaces

The possibility to determine both the spin and orbital moments (denoted as $\langle S_z \rangle$ and $\langle L_z \rangle$, respectively) directly from x-ray magnetic circular dichroism (MCD, Schütz et al., 1987; Stöhr, 1993, 1995) spectra by applying recently proposed simple but powerful MCD sum rules has attracted considerable excitement and attention (Thole et al., 1992; Carra et al., 1993). Since these sum rules have been derived from a single ion model, their validity for complex materials (e.g., transition metals) with strong multi-shell hybridization (excluded in the original derivation) needs to be verified. As is well known, MCD measures the difference in absorption between right- and left-circularly polarized incident light during the process of electric transitions from core states to unoccupied valence states. Due to the spin-orbit coupling between valence states, the MCD signals of σ_m $(= \sigma_+ - \sigma_-)$ for the L_2 and L_3 absorption edge for $3d$ transition metals no longer cancel each other as they do in the absence of SOC where the integrated L_2 and L_3 signals are equal and opposite. Here, σ_+ and σ_- represent the absorption cross sections for left- and right-circularly polarized light, respectively.

As stated in the MCD sum rules, integrations of the MCD and total absorption spectra relate directly to $\langle L_z \rangle$, $\langle S_z \rangle$ and $\langle T_z \rangle$ for the unoccupied states

$$\frac{I_m}{I_t} = \frac{\int_{L_3+L_2} \sigma_m dE}{\int_{L_3+L_2} \sigma_t dE} = \frac{\langle L_z \rangle}{2N_h} \; ; \quad N_h = \int \rho(E) dE \tag{11}$$

and

$$\frac{I_s}{I_t} = \frac{\int \sigma_s dE}{I_t} = \frac{\int (\sigma_{m,L_3} - 2\sigma_{m,L_2}) dE}{\int_{L_3+L_2} \sigma_t dE} = \frac{\langle S_e \rangle}{N_h} = \frac{\langle S_z \rangle + 7\langle T_z \rangle}{3N_h} \, , \tag{12}$$

where $\sigma_m = \sigma_+ - \sigma_-$ and $\sigma_t = \sigma_+ + \sigma_- + \sigma_z$. $\mathbf{T}$ is the spin magnetic dipole operator, i.e., $\mathbf{T} = \frac{1}{2}[\mathbf{S} - 3\hat{\boldsymbol{r}}(\hat{\boldsymbol{r}} \cdot \mathbf{S})]$, $(T_z = S_z(1 - 3\cos^2\theta)/2$ for $\mathbf{S}$ aligned along the z direction). The number of valence holes, N_h, can be obtained from an integration over the unoccupied density of states $(\rho(E))$.

There are two assumptions in the derivation of the sum rules: (i) the radial matrix elements are constant for all transitions, and (ii) no hybridization exists between different l shells (i.e., l is a good quantum number). As is well-known, both assumptions fail in real materials and thus weak s,p–d hybridization (which

Table II. Calculated values of $\langle L_z \rangle$, $\langle S_z \rangle$, $\langle T_z \rangle$, $\langle S_e \rangle$ and N_h and sum rule errors $R_1 = \frac{I_m}{I_t} / \frac{\langle L_z \rangle}{2N_h} - 1$, $R_2 = \frac{I_s}{I_t} / \frac{\langle S_e \rangle}{N_h} - 1$ and $R_3 = \frac{I_m}{I_s} / \frac{\langle L_z \rangle}{2S_e} - 1$ for Ni(001), Co(0001) and Fe(001) surface (S) and bulk-like centre (C) layers.

Atom	$\langle L_z \rangle$	$\langle S_z \rangle$	$7\langle T_z \rangle$	$\langle S_e \rangle$	N_h	R_1	R_2	R_3
Ni(S)	−0.069	−0.67	−0.082	−0.250	1.81	0.27	0.52	−0.10
Ni(C)	−0.051	−0.62	−0.027	−0.215	1.66	0.20	0.36	−0.11
Co(S)	−0.090	−1.61	0.240	−0.457	2.60	0.11	0.24	−0.09
Co(C)	−0.078	−1.52	0.014	−0.502	2.55	0.09	0.22	−0.10
Fe(S)	−0.111	−2.71	0.230	−0.828	3.70	0.10	0.16	−0.04
Fe(C)	−0.063	−2.10	0.028	−0.691	3.34	0.04	0.15	−0.09

affects both assumptions) is important for the validity of the sum rule. Since the effects of s,p states are inherent in real materials and thus in the experimental spectra, the validity of these sum rules needs to be checked. To this end, FLAPW calculations were carried out to obtain both the MCD spectra (I_m, I_s and I_t) and ground state properties ($\langle S_z \rangle$, $\langle L_z \rangle$, $\langle T_z \rangle$ and N_h).

In a series of investigations (Wu et al., 1993; 1994), we found that the main mechanism affecting the validity of the sum rules is the hybridization between the d states and the high-lying s,p states. Significantly, the I_t and N_h are not well defined quantities since they do not converge with respect to the upper-limit of the energy integration, and thus an arbitrary energy cut-off has to be applied in order to stay within the d band region. Thus, we proposed a criterion for the choice of the energy cut-off, i.e., cut the integrations for I_t and N_h at the energy where the MCD counterpart becomes acceptably close to zero. Based on this criterion, we adopted an energy cut-off of 6 eV above E_F for the calculated results for Fe, Co and Ni (bulk and surfaces).

As listed in Table II, the validity of the spin and orbital sum rules is denoted by $R_1 = \frac{I_m}{I_t} / \frac{\langle L_z \rangle}{N_h} - 1$, and $R_2 = \frac{I_s}{I_t} / \frac{\langle S_e \rangle}{N_h} - 1$. Obviously, the orbital sum rule is seen to work very well (within 10%) for Fe and Co systems, and the error becomes larger for Ni since the number of s,p holes is almost equal to that of d holes (we used an energy cutoff of 6 eV above E_F). By contrast, the errors of the spin sum rule are much larger; it actually fails severely for the Ni surface since R_2 is as large as 52%.

In addition, the $\langle T_z \rangle$ term in the spin sum rule is negligible only for atoms with cubic symmetry. For atoms in non-cubic environments such as surfaces and interfaces, as seen from Table II, its importance is obvious, since its magnitude becomes 8.5%, 12% and 15% of $\langle S_z \rangle$ at E_F for Fe(001), Ni(001) and Co(0001),

respectively. The hybridization between different l shells is the main mechanism causing the failure of the MCD spin sum rule for transition metals. Without s,p states, the error of the MCD spin sum rule can be reduced to within 10% even for the Ni surface.

We have emphasized the need for a proper energy cut-off for the integrations in order to eliminate the error introduced by the high lying s,p states through the normalizing denominators. A better way is to combine the $\langle L_z \rangle$ and $\langle S_z \rangle$ sum rules, as was done recently in some experiments on bulk transition metals. From our first principles calculations, we found that the error in the ratio $R_3 = \frac{I_m}{I_s} / \frac{\langle L_z \rangle}{\langle S_e \rangle} - 1$, is 10% or so for all systems studied.

8 Conclusions

In summary, state-of-the-art *ab initio* LSD electronic structure calculations have achieved great success in the exciting field of thin film magnetism, in both explaining existing phenomena and, more importantly, in predicting the properties of new systems. Illustrative results demonstrate that: (1) the lowered coordination number at clean metal surfaces leads to enhanced magnetic moments; (2) noble metal and MgO substrates do not affect the magnetism in most cases, but show significant effects on 4*d* overlayers; (3) the strong interaction (hybridization) with nonmagnetic transition metals diminishes (entirely in some cases) the ferromagnetism and usually leads to AFM ordering; (4) the magnetic anisotropy and magnetostriction can be predicted correctly using the state-tracking and torque procedures; and (5) x-ray magnetic circular dichroism can be explained in the framework of interband transitions. In the future, electronic structure theory is expected to continue to play a predictive role by considering more practical systems, by eliminating the limitation of the local spin density approximation and developing more efficient and precise methods.

9 Acknowledgement

This work is dedicated to the memory of Allan Mackintosh, an outstanding physicist and a close friend of one of us (AJF). He will be missed. Work supported by the ONR (Grant Nos. N00014-95-1-0489 and N00014-94-1-0030) and by a computing grant at the Arctic Region Supercomputing Center and at the National Energy Research Supercomputing Center (NERSC) supported by the DOE.

References

Baberschke K, 1996: Appl. Phys. A **62**, 417
Baibich MN, Broto JM, Fert A, Dau A, Petroff F, Eitenne P, Creuzet G, Friederich A, and Chazelas J, 1988: Phys. Rev. Lett. **61**, 2472
Binasch G, Grunberg P, Saurenbach F and Zinn W, 1989: Phys. Rev. B **39**, 4828
Carra P, Thole BT, Altarelli M and Wang XD, 1993: Phys. Rev. Lett. **70** 694
Carcia PA, Meinholdt AD and Suna A, 1985: Appl. Phys. Lett. **47**, 178
Daughton JM, 1992: Thin Solid Films, **216**, 162
Dieny B, Speriosu VS, Parkin SSP, Gurney AB, Wilhoit DR and Mauri D, 1991: Phys. Rev. B **43**, 1279
Freeman AJ and Wu RQ, 1991: J. Magn. Magn. Mater. **100**, 497
Hurst JE Jr. and Kozlovsky WJ, 1993: Jpn. J. Appl. Phys. **32**, 5301
Liu C and Bader SD, 1992: Phys. Rev. B **44**, 12056
Mulhollan GA, Fink RL and Erskine JL, 1991: Phys. Rev. B **44**, 2393
Parkin SSP, More N and Roche KP, 1990: Phys. Rev. Lett. **64**, 2304
Pfandzelter R, Steierl G and Rau C, 1995: Phys. Rev. Lett. **74**, 3467
Roth C, Kleeman Th, Hillebrecht FU and Kisker E, 1995: Phys. Rev. B **52**, 15691
Schütz G, Wagner W, Wilhelm W, Kienle P, Zeller R and Materlik G, 1987: Phys. Rev. Lett. **58**, 737
Stöhr J, 1993: Science **259**, 658
Stöhr J, 1995: J. Electron Spectroscopy and Rel. Phenom. **75**, 253
Thole BT, Carra P, Sette F and Van der Laan G, 1992: Phys. Rev. Lett. **68** 1943
Wang DS, Wu RQ and Freeman AJ, 1993: Phys. Rev. Lett. **70**, 869
Wang XD, Wu RQ, Wang DS and Freeman AJ, 1996: Phys. Rev. B **54**, 61
Wimmer E, Krakauer H, Weinert M and Freeman AJ, 1981: Phys. Rev. B **24**, 864
Wu RQ and Freeman AJ 1992, Phys. Rev. B. **45**, 7222
Wu RQ, Wang DS and Freeman AJ, 1993: Phys. Rev. Lett. **71** 3581
Wu RQ and Freeman AJ, 1994: Phys. Rev. Lett. **73** 1994
Zhu MJ, Bylander DM and Kleinman L, 1990: Phys. Rev. B **42**, 2874